JCI insight

# TLR9/MyD88/TRIF signaling activates host immune inhibitory CD200 in *Leishmania* infection

Ismael P. Sauter, … , Wadih Arap, Mauro Cortez

*JCI Insight.* 2019;4(10):e126207. https://doi.org/10.1172/jci.insight.126207.

Research Article | Infectious disease

## Graphical abstract

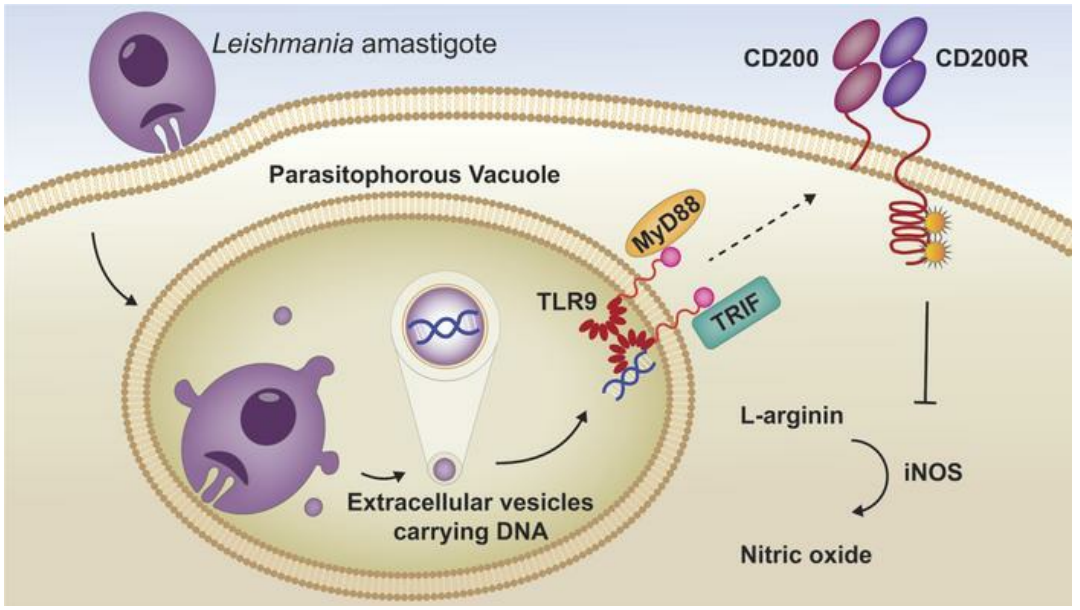

JCI insight

RESEARCH ARTICLE

# TLR9/MyD88/TRIF signaling activates host immune inhibitory CD200 in *Leishmania* infection

**Ismael P. Sauter,[1] Katerine G. Madrid,[1] Josiane B. de Assis,[2] Anderson Sá-Nunes,[2] Ana C. Torrecilhas,[3] Daniela I. Staquicini,[4] Renata Pasqualini,[4] Wadih Arap,[5] and Mauro Cortez[1]**

[1]Department of Parasitology and [2]Department of Immunology, Institute of Biomedical Sciences, University of São Paulo, São Paulo, Brazil. [3]Department of Pharmaceutical Sciences, Federal University of São Paulo, São Paulo, Brazil. [4]Rutgers Cancer Institute of New Jersey and Division of Cancer Biology, Department of Radiation Oncology, Rutgers New Jersey Medical School, Newark, New Jersey, USA. [5]Rutgers Cancer Institute of New Jersey and Division of Hematology/Oncology, Department of Medicine, Rutgers New Jersey Medical School, Newark, New Jersey, USA.

**Virulent protozoans named *Leishmania* in tropical and subtropical areas produce devastating diseases by exploiting host immune responses. Amastigotes of *Leishmania amazonensis* stimulate macrophages to express CD200, an immunomodulatory ligand, which binds to its cognate receptor (CD200R) and inhibits the inducible nitric oxide synthase and nitric oxide (iNOS/NO) signaling pathways, thereby promoting intracellular survival. However, the mechanisms underlying CD200 induction in macrophages remain largely unknown. Here, we show that phagocytosis-mediated internalization of *L. amazonensis* amastigotes following activation of endosomal TLR9/MyD88/TRIF signaling is critical for inducing CD200 in infected macrophages. We also demonstrate that *Leishmania* microvesicles containing DNA fragments activate TLR9-dependent CD200 expression, which inhibits the iNOS/NO pathway and modulates the course of *L. amazonensis* infection in vivo. These findings demonstrate that *Leishmania* exploits TLR-signaling pathways not only to inhibit macrophage microbicidal function, but also to evade host systemic immune responses, which has many implications in the severity of the disease.**

## Introduction

Macrophages initiate the innate immune response against parasitic infections. After detecting parasites, signaling pathways triggered by the interaction of pathogen-associated molecular patterns (PAMPs) with Toll-like receptors (TLRs) are activated in macrophages, leading to pathogen elimination and recruitment of immune cells to restrain the remaining infection and inflammation (1, 2). Throughout the infection period, a delicate balance between activating and controlling the immune system preserves the integrity of the host to restore homeostasis. Yet, many pathogens have evolved to exploit these control mechanisms to escape host defenses and establish infection. The protozoan parasite *Leishmania*, which causes various clinical forms of leishmaniasis, constitutes a prime example of a pathogen that successfully adapted to live inside macrophages, thereby escaping their inherent cellular antimicrobial attributes (3, 4). Several clinically relevant models are available (5) including inbred and deficient mice (6) that allow studying all steps of the disease, from infection to the progression of lesions and ultimately death.

Leishmaniasis comprises a range of tropical diseases that cause cutaneous, mucocutaneous, and visceral pathologies in humans and other animals (7, 8). *Leishmania* parasites are transmitted by infected hematophagous female sandflies (9). Parasite-host interactions are multifaceted, involving several pathogenicity factors for host immune responses and different species of *Leishmania*. In Brazil, *Leishmania amazonensis* is known to be the causative agent of cutaneous and diffuse cutaneous leishmaniasis (10). It was demonstrated that these parasites inhibit innate immune responses and promote their virulence by inducing expression of CD200 (also known as the OX-2 membrane glycoprotein), an immunoregulatory molecule that downregulates the leishmanicidal response of macrophages (11).

CD200 and its cognate receptor (CD200R) are cell surface glycoprotein members of the immunoglobulin superfamily. CD200 is broadly expressed in many cell types, including thymocytes, B cells, activated T cells,

**Conflict of interest:** The authors have declared that no conflict of interest exists.



**Submitted:** November 14, 2018
**Accepted:** April 11, 2019
**Published:** May 16, 2019.

**Reference information:** *JCI Insight*. 2019;4(10):e126207. https://doi.org/10.1172/jci.insight.126207.

neurons, and endothelial cells (12–14). On the other hand, CD200R expression is limited to myeloid cells and specific T cell populations (15–17). Activation of CD200R by CD200 suppresses the inflammatory response of macrophages and cytotoxic T cells, which induces tolerance and activates regulatory T cells (18, 19). During *L. amazonensis* infection, expression of CD200 in murine macrophages supports the growth of intracellular amastigotes by downregulating nitric oxide (NO) production by inducible nitric oxide synthase (iNOS), the main mechanism of parasite control (11, 20, 21). However, these reports did not reveal the molecular machinery that triggers these responses. We hypothesized that *L. amazonensis* activates TLR-mediated signaling to increase parasite virulence in experimental models.

## Results

*CD200 expression requires phagocytosis-mediated internalization*. Amastigotes of *L. amazonensis* induce expression of CD200 in bone marrow macrophages (BMMs) at early stages of the host cell–parasite interaction (11). Notably, axenic amastigotes, which are obtained from axenic culture, and lesion amastigotes obtained from cutaneous lesions of infected mice, induced similar levels of CD200 expression in infected BMMs (Figure 1A), as shown by tandem immunoprecipitation (IP) followed by Western blot analysis with a specific anti-CD200 antibody. To investigate whether parasite attachment or internalization triggers intracellular inhibitory signaling pathways mediated by CD200 expression, we used BMMs derived from C57BL/6 mice treated or not with cytochalasin D (Cyto-D), a drug that affects actin polymerization and inhibits phagocytosis (22). We noted a marked inhibition of CD200 expression in BMMs treated with Cyto-D and infected with *L. amazonensis* amastigotes. We observed high CD200 expression in infected and nontreated BMMs (Figure 1B). In contrast, noninfected BMMs and noninfected BMMs treated with Cyto-D showed only basal levels of CD200 expression. To evaluate the effect of actin polymerization on cell invasion, we determined the number of intracellular parasites per infected cell compared to the number of parasites attached but not internalized. We identified attached parasites from internalized parasites under immunofluorescence (IF) analysis in nonpermeabilized infected cells. In this assay, attached parasites were stained with a polyclonal anti-*Leishmania* antibody followed by a secondary fluorophore-conjugated antibody (green), while only the nuclei and kinetoplasts of internalized parasites showed propidium iodide staining (red), as seen in Figure 1C. Treatment with Cyto-D reduced the number of internalized amastigotes by approximately 40% in BMMs, whereas it increased the number of attached parasites (Figure 1D), showing no effect on the total number of parasites associated with BMMs (Figure 1E). Because phagocytosis is an active process in macrophages that promotes internalization of parasites either live or dead, we reasoned that parasite viability would require inducing CD200 expression in BMMs. To address this possibility, we next incubated BMMs with live or dead amastigotes of *L. amazonensis*. We employed 2 different methods to kill the parasites: fixing with paraformaldehyde (PFA) or heating at 65°C degrees for 45 minutes. Parasite viability after treatment is shown in Supplemental Figure 1; supplemental material available online with this article; https://doi.org/10.1172/jci.insight.126207DS1. We only observed phagocytosis-induced CD200 expression in BMMs infected with live parasites (Figure 1F), despite the similar percentages of phagocytosed live and dead parasites (Figure 1, G and H). These results indicate that phagocytosis of live amastigotes is essential for activating intracellular pathway(s) that ultimately induce CD200 expression in BMMs infected by *L. amazonensis*.

*Endosomal TLR9/MyD88/TRIF activation induces CD200 expression*. Among the TLRs involved in innate immune responses against *Leishmania* spp., the most studied are TLR2 and TLR4 localized on the cellular plasma membrane and TLR3 and TLR9 localized on the membrane of endosomal compartments (23). To investigate whether induced CD200 expression is associated with downstream signaling pathways activated by TLRs, we treated BMMs with specific agonists: gram-positive bacterial peptidoglycan (PGN, a TLR2 agonist), polyinosinic-polycytidylic acid (poly I:C, a TLR3 agonist), gram-negative bacterial lipopolysaccharide (LPS, a TLR4 agonist), and unmethylated CpG motifs (CpG, a TLR9 agonist). We observed a marked and specific increase in the levels of CD200 expression only after treatment with the TLR9 agonist CpG (Figure 2A). This effect is confirmed by densitometric analysis of the bands (CD200/actin ratio). Indeed, the CpG-induced CD200 expression in BMMs occurred as early as 60 minutes after incubation, which corresponded to BMMs infected with amastigotes of *L. amazonensis* (11).

While TLRs expressed on the plasma membrane recognize surface PAMPs, endosomal TLRs recognize primarily microbial nucleic acids (24, 25). To evaluate whether *L. amazonensis* amastigotes induce CD200 expression through TLR activation, we used BMMs derived from TLR2-null, TLR3-null, TLR4-null, and

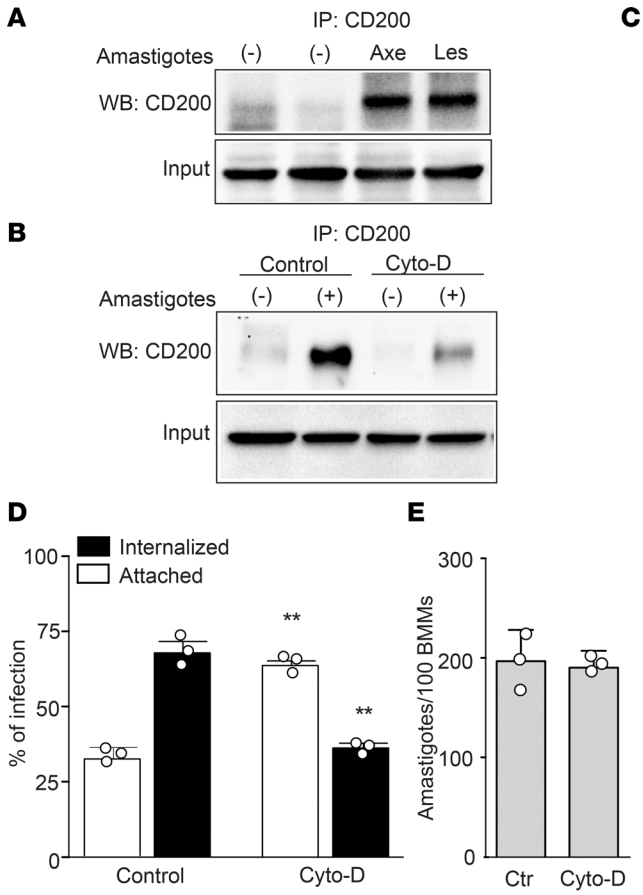
A
IP: CD200
Amastigotes (-) (-) Axe Les
WB: CD200
Input
B
IP: CD200
Control Cyto-D
Amastigotes (-) (+) (-) (+)
WB: CD200
Input
D
Internalized
Attached
% of infection
100
75
50
25
0
**
**
Control
Cyto-D
E
Amastigotes/100 BMMs
300
200
100
0
Ctr
Cyto-D

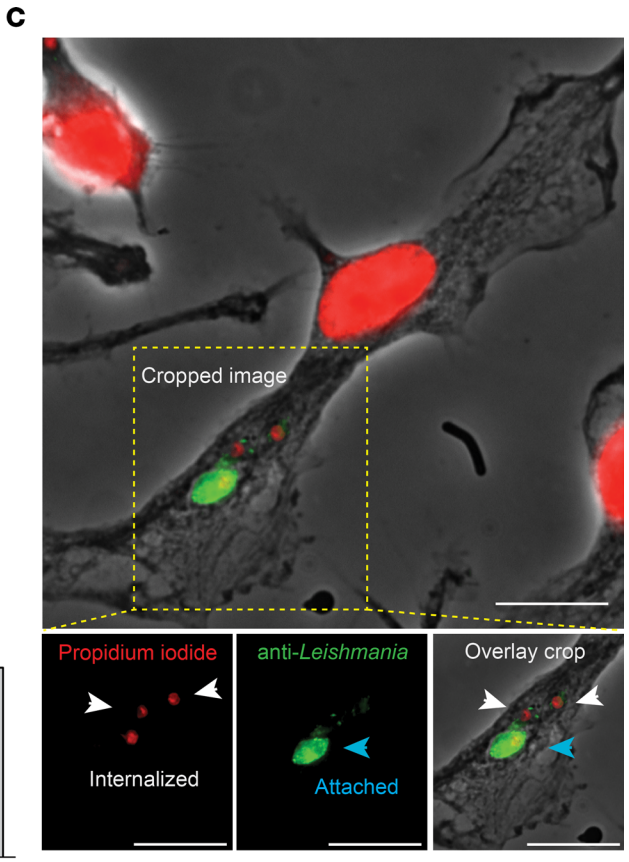
C
Cropped image
Propidium iodide
Internalized
anti-Leishmania
Attached
Overlay crop

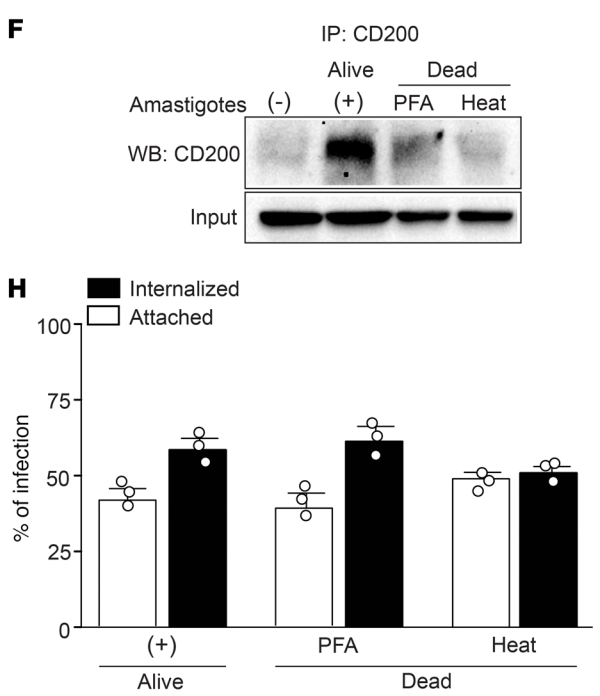
F
IP: CD200
Alive Dead
Amastigotes (-) (+) PFA Heat
WB: CD200
Input
H
Internalized
Attached
% of infection
100
75
50
25
0
(+)
PFA
Heat
Alive
Dead

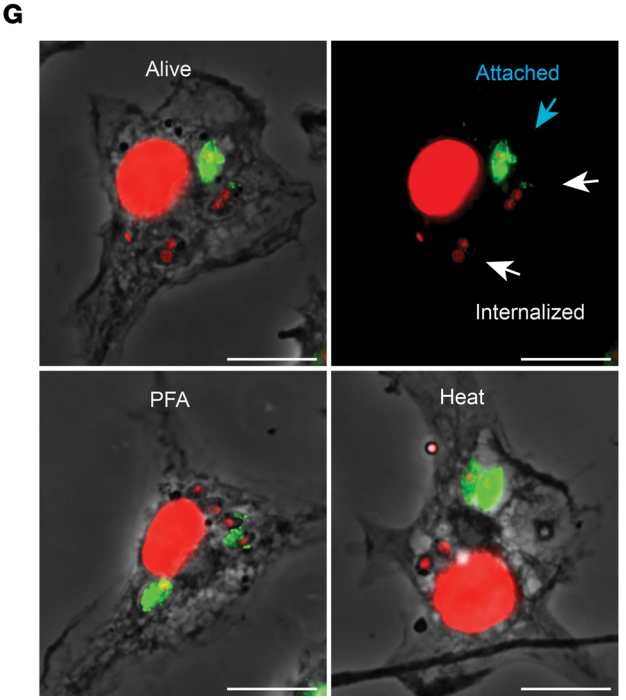
G
Alive
Attached
Internalized
PFA
Heat

**Figure 1. Macrophage CD200 expression induced by *Leishmania amazonensis* requires phagocytosis of viable parasites.** (**A**) BMMs infected with axenic (Axe) or lesion (Les) amastigotes of *L. amazonensis* for 1 hour. (**B**) BMMs pretreated with cytochalasin D (Cyto-D) and infected (+) or not (–) with lesion amastigotes for 1 hour. CD200 protein levels analyzed by IP/Western blot. Actin from IP-input sample served as loading control. (**C**) Representative immunofluorescence images of the amastigote in vitro infection, showing attached (blue arrowheads) or internalized (white arrowheads) parasites. Amastigotes were stained sequentially with anti-*Leishmania* antibodies and anti–rabbit IgG Alexa Fluor 488 (green). Nuclei were stained with propidium iodide (red). (**D**) Percentage of the attached (white bars) or internalized (black bars) amastigote infection after Cyto-D treatment in BMMs. Results correspond to the mean ± SD of 3 independent experiments. $^{**}P < 0.01$ (2-way ANOVA). (**E**) Total number of amastigotes in infected BMMs pretreated or not with cytochalasin. The data correspond to the mean ± SD of triplicates. Results expressed as amastigotes per 100 infected BMMs representative of 3 independent experiments. (**F**) IP/Western blot of CD200 in samples from BMMs incubated with live or dead amastigotes (either by PFA or heat treatment). (**G**) Representative images of BMMs incubated with live or dead amastigotes and processed as in **C**. Scale bars: 10 μm (**C** and **G**). (**H**) Percentage of infection for attached (white bars) or internalized (black bars) amastigotes for the in vitro assay shown in **E**. At least 300 cells per coverslip were counted for each assay. Results correspond to the mean ± SD of 3 independent experiments.

TLR9-null mice. We detected high CD200 expression in infected BMMs derived from wild-type (WT), *TLR2*$^{-/-}$, *TLR3*$^{-/-}$, and *TLR4*$^{-/-}$ mice, whereas we observed no induction of CD200 expression in *TLR9*$^{-/-}$-derived BMMs (Figure 2B). Among the tested BMMs, we found no significant differences in the percentage of infection (Supplemental Figure 2) or in the number of parasites per infected cell after 1 hour (Figure 2C).

The TLR-associated signaling cascade is dependent on recruitment of 2 major adaptor proteins: MyD88 and TRIF (26). Although TLR9 activation promotes recruitment and signaling outcomes through recruiting MyD88, TRIF can serve as an alternative signaling route via TLR9 (27). To evaluate these TLR adaptor proteins in *L. amazonensis*–induced CD200 expression, we used BMMs derived from WT, MyD88-null (*MyD88*$^{-/-}$), or TRIF-null (*TRIF*$^{-/-}$) mice in infection assays, which showed no difference in the number of intracellular parasites after 1 hour of infection (Figure 2D). We only detected CD200 expression in infected BMMs from WT mice, not in BMMs from *MyD88*$^{-/-}$ or *TRIF*$^{-/-}$ mice (Figure 2E). These data show that parasite internalization is not affected by the absence of MyD88 or TRIF and suggest that TLR9-induced CD200 expression requires both adaptor proteins, MyD88 and TRIF. Taken together, the data indicate that intracellular parasites engage TLR9 signaling pathways through MyD88 and TRIF to induce expression of CD200 in BMMs upon infection with *L. amazonensis* amastigotes.

*TLR9-dependent CD200 expression inhibits iNOS/NO microbicidal responses*. TLR9 recognizes unmethylated CpG DNA sequences (28, 29). To investigate TLR9 activation by *L. amazonensis*, we incubated BMMs from WT mice with different concentrations of total DNA purified from amastigotes and analyzed CD200 expression. We observed elevated expression of CD200 in macrophages incubated with 1 μg/ml of total parasite DNA (Figure 3A). Since the signaling pathways triggered by TLR9 induce expression of CD200, we hypothesized that TLR9 activation by *L. amazonensis* DNA would inhibit iNOS expression and NO production. Therefore, we primed BMMs with LPS and then incubated them with either the parasite (*L.a*) or purified parasite DNA (*L.a* DNA). We then analyzed the levels of iNOS and NO. As a control, we used recombinant CD200-Fc, which inhibits iNOS expression (11, 30). Purified *L. amazonensis* DNA inhibited iNOS expression in LPS-activated macrophages (Figure 3B) and NO production (Figure 3C) to similar levels after exposure to intracellular parasites or recombinant CD200-Fc. To correlate the involvement of TLR9 signaling and the iNOS/NO mechanism, we analyzed the levels of iNOS transcripts at initial time points of *Leishmania* infection in macrophages from WT and *TLR9*$^{-/-}$ mice by quantitative PCR (qPCR). Interestingly, an opposite response of iNOS transcripts was observed between WT and *TLR9*$^{-/-}$ infected macrophages. While iNOS transcripts decreased from 1 hour to 3 hours of infection in macrophages from WT mice, the levels of these transcripts were significantly higher after 3 hours in *TLR9*$^{-/-}$ infected macrophages, suggesting that without TLR9, induction of CD200 expression is inhibited, and consequently the levels of iNOS increase, favoring parasite elimination (Figure 3D). To verify that *TLR9*$^{-/-}$ BMMs are responsive to iNOS, we verified the production of nitrite in WT and *TLR9*$^{-/-}$ macrophages activated by LPS or CpG agonists. As expected, WT and *TLR9*$^{-/-}$ macrophages produced nitric oxide when stimulated with both agonists, with slightly higher production in *TLR9*$^{-/-}$ macrophages stimulated with LPS (Figure 3E). However, this effect is drastically inhibited in the presence of recombinant CD200-Fc (Figure 3F), indicating that TLR9 is directly associated with the expression of CD200, but independent of the iNOS/NO inhibition induced by this ligand. Because CpG induced CD200 expression in macrophages (Figure 2A), we expected a similar inhibitory effect on nitric oxide production. However, CpG increased the levels of nitrite, suggesting that parasite DNA and CpG induce signaling pathways through TLR9 that results in CD200 expression. Importantly, CD200 induced by CpG is not involved in macrophage iNOS/NO inhibition. These results suggest that

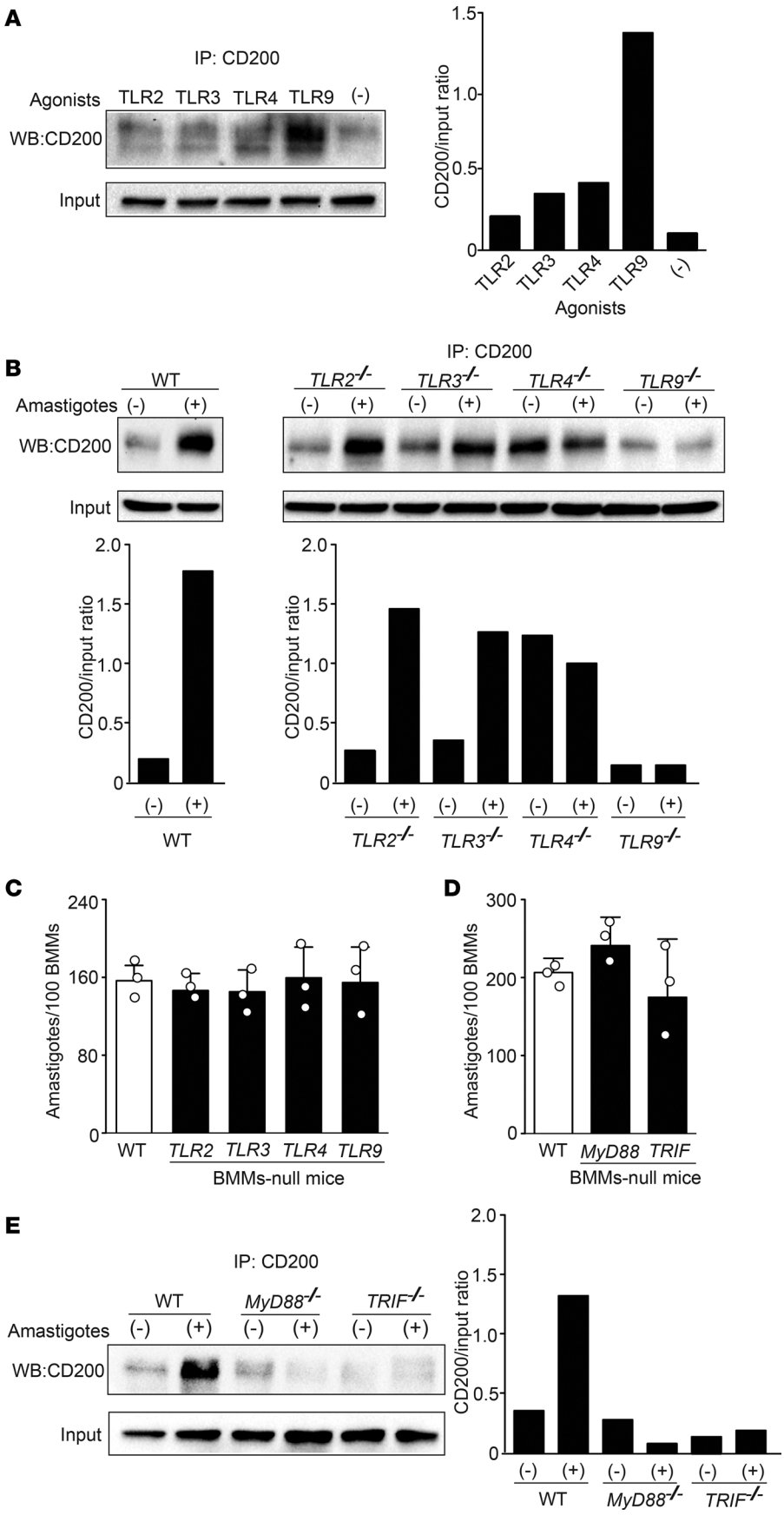


**Figure 2. *Leishmania amazonensis*–induced CD200 expression requires TLR9, MyD88, and TRIF signaling pathways in macrophages infected with amastigotes.** (**A**) A TLR9 agonist induces significant upregulation of CD200. IP followed by Western blot (WB) of CD200 performed in BMMs stimulated for 1 hour with different TLR agonists: TLR2 (peptidoglycan), TLR3 (poly I:C), TLR4 (LPS), and TLR9 (CpG). WB with an actin mAb was used as a sample input control. Densitometric analysis of CD200/actin input ratio is presented in every WB. (**B**) BMMs from WT and TLR-deficient mice were infected for 1 hour with amastigotes, lysed, and subjected to CD200 IP/Western blot. (**C**) The number of amastigotes in infected BMMs from WT compared with BMMs from *TLR*$^{-/-}$ mice or (**D**) *MyD88*$^{-/-}$ and *TRIF*$^{-/-}$ mice. The data correspond to the mean ± SD of triplicates. Results expressed as amastigotes per 100 infected BMMs representative of 3 independent experiments and at least 300 cells per coverslip were counted for each assay. (**E**) Level of CD200 expression analyzed as in **B** in infected BMMs from WT and *MyD88*$^{-/-}$ and *TRIF*$^{-/-}$ mice. Densitometric analysis of CD200/actin input ratio is presented on the right.

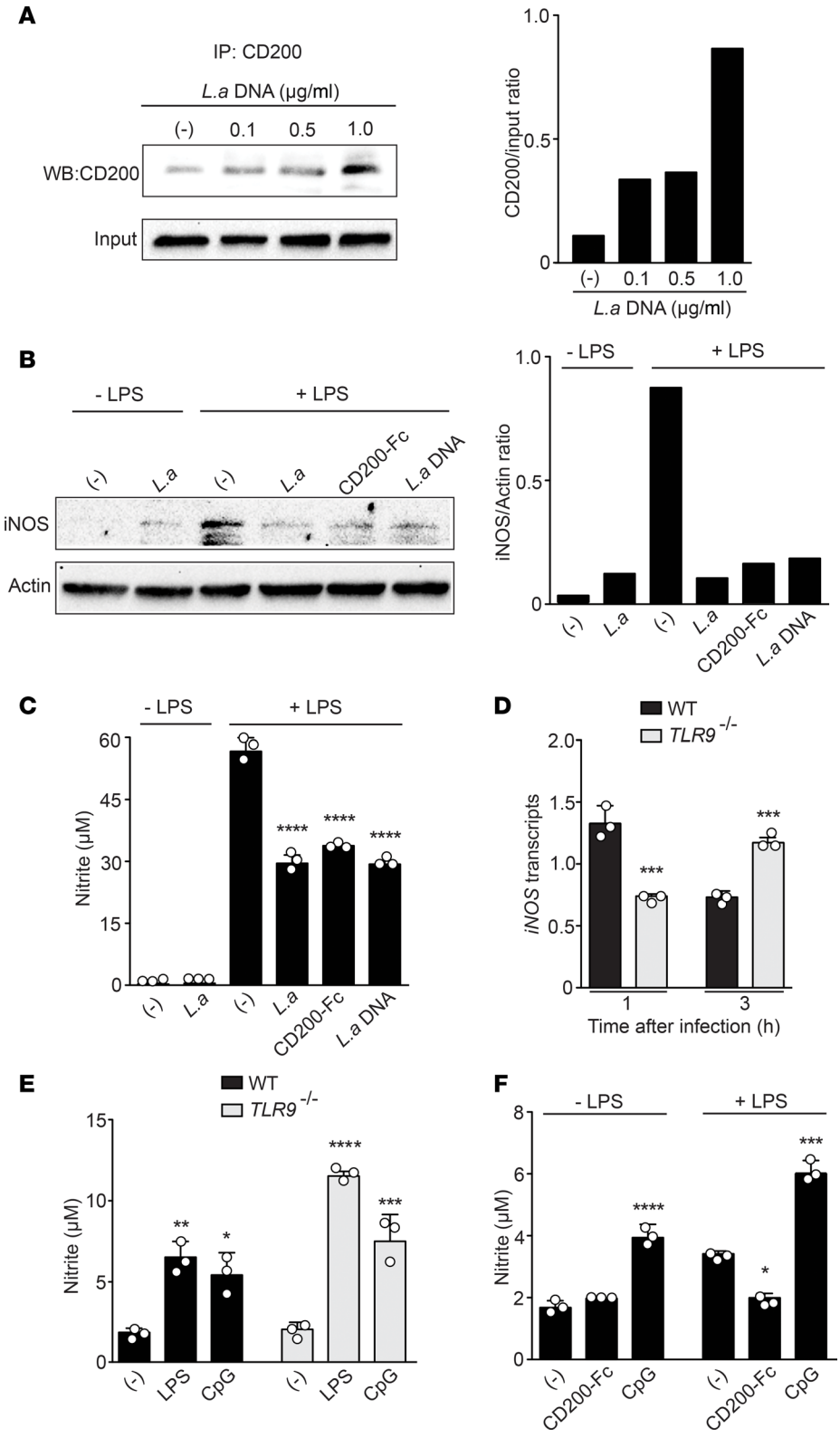


**Figure 3. Parasite DNA induces host CD200 and downregulates iNOS/NO.** (**A**) CD200 protein levels in BMMs stimulated for 1 hour with different concentrations of *Leishmania amazonensis* DNA (0.1, 0.5, and 1 μg/ml) and densitometric analysis using CD200/actin input ratio. (**B**) Expression of iNOS in the protein extract from untreated or LPS-treated BMMs and infected with amastigotes (*L.a*) or treated with CD200-Fc (2 μg/ml) or with amastigotes-DNA (1 μg/ml). Densitometric analysis of iNOS/actin ratio is presented on the right. (**C**) NO levels in the supernatant of BMMs treated and processed as in **B**. Results correspond to the mean ± SD of triplicates. ***$P < 0.001$ (2-way ANOVA). (**D**) iNOS transcript levels determined by qPCR in BMMs from WT and *TLR9*$^{-/-}$ mice infected for 1 or 3 hours with axenic amastigotes of *L. amazonensis*. The data correspond to the mean ± SD of triplicates. ***$P < 0.0002$ (Student's *t* test). (**E**) NO levels in the supernatant of BMMs from WT and *TLR9*$^{-/-}$ mice treated with LPS or CpG (1 μg/ml) and incubated for 24 hours. Results correspond to the mean ± SD of triplicates. WT: (–) vs. LPS, **$P = 0.0017$; (–) vs. CpG, *$P = 0.0175$; *TLR9*$^{-/-}$: (–) vs. LPS, ****$P < 0.0001$; (–) vs. CpG, ***$P = 0.0006$ (2-way ANOVA). (**F**) NO levels in the supernatant of LPS-treated BMMs and treated with CD200-Fc (2 μg/ml) or CpG (1 μg/ml) and incubated for 24 hours. Results correspond to the mean ± SD of triplicates. Untreated: (–) vs. CpG, ***$P < 0.0001$; +LPS: (–) vs. CD200Fc, *$P = 0.0394$; (–) vs. CpG, ****$P < 0.0001$ (2-way ANOVA).

DNA of *L. amazonensis* amastigotes specifically inhibits the iNOS/NO pathway by inducing TLR9-dependent CD200 expression in BMMs.

*L. amazonensis amastigote–secreted EVs induce host CD200.* Several reports have demonstrated secretion of extracellular vesicles (EVs) in different species of *Leishmania* (31–33). These vesicles can be classified into microvesicles (mVEs: 100–1000 nm) or exosomes (40–100 nm) according to their size and density (34, 35).

Parasite-derived EVs carrying active proteins and nucleic acids can have modulatory effects in macrophage signaling and function (33, 36, 37). Given the similarities in EV contents in vivo and in vitro (38), we investigated TLR9 activation by EVs secreted by axenic amastigotes of *L. amazonensis*. To evaluate EV shedding, we incubated parasites in culture media for 2 hours followed by scanning and transmission electron microscopy (SEM and TEM, respectively). We analyzed the supernatant containing secreted EVs by nanoparticle tracking analysis (NTA). As predicted, we observed numerous amastigote-associated EVs (arrows) budding from different locations on the surface of the parasite plasma membrane by SEM (Figure 4A) and TEM (Figure 4B). By NTA analysis, we observed that EVs recovered from the supernatant were mostly composed of mVEs varying from 94 nm to 216 nm in diameter (Figure 4C). Next, we loaded *L. amazonensis* amastigotes with carboxytetramethylrhodamine (TAMRA), a rhodamine-based fluorescent dye, and performed time-lapse mVE release experiments during BMM infection. By using confocal microscopy, we visualized punctate fluorescence corresponding to released mVEs (white arrowhead) at early time points of parasite contact with the macrophages (Figure 4, D and E). This time period corresponds to the rapid induction of CD200 in infected BMMs.

We then evaluated this vesicle budding mechanism in TLR9-induced CD200 expression. We purified the DNA content from mVEs (DNA-mVEs) from cultured amastigotes and added it to BMMs from WT mice. We used intact mVEs and CpG as controls. DNA-mVEs and intact mVEs induced CD200 expression to levels seen with the TLR9 agonist CpG by Western blot and confirmed with densitometric analysis (Figure 4F). These data show that DNA-containing mVEs secreted by amastigotes of *L. amazonensis* activate TLR9, which in turn induces CD200 expression and inhibits iNOS and NO production in macrophages. Together, these results provide mechanistic evidence for intracellular activation of TLR9 by *L. amazonensis* amastigote–secreted mVEs.

*TLR9 activation modulates L. amazonensis virulence in vivo*. To evaluate the induced CD200 expression by TLR9 activation in vivo, we followed the progression of cutaneous lesions in the footpads of WT and *TLR9*$^{-/-}$ mice infected with *L. amazonensis*. We have previously demonstrated that *CD200*$^{-/-}$ mice are resistant to *L. amazonensis* infection and develop small cutaneous lesions containing fewer parasites than control mice (11). As early as the third week of infection, infected *TLR9*$^{-/-}$ mice developed much smaller lesions, containing a reduced number of parasites recovered at the end of the experiment (Figure 5, A–C, and Supplemental Figure 3A). As expected, WT mice showed rapidly growing and nonhealing lesions typical of *L. amazonensis* infection (Figure 5, A and B) that had an increased parasite load in the infected tissue (Figure 5C) relative to mild infection observed in *TLR9*$^{-/-}$ mice. Because of the remarkable difference in the progression of lesions observed between WT and *TLR9*$^{-/-}$ mice, we sought to compare the inflammatory response in the footpad lesions by determining the cytokine profile in each animal group. A tendency towards an inflammatory profile was observed in samples from *TLR9*$^{-/-}$ mice, with at least 3-fold more IL-12p70 and significantly low levels of the antiinflammatory IL-4 and IL-10 cytokines in comparison with WT mice (Figure 5D). Other cytokines such as IL-1β, TNF-α, IL-12p40, IL-6, and IFN-γ were either not significantly altered or undetectable (Supplemental Figure 3B).

One might suggest that such results have occurred due to the early phase of *L. amazonensis* infection. We did detect an antiinflammatory-like immune response (IL-12$^{lo}$, IL-4$^{hi}$, IL-10$^{hi}$), which correlates with the TLR9-mediated CD200 phenotype. This cytokine profile was previously reported in *L. amazonensis* infection (39). At the fifth week of *Leishmania* infection, lesion progression intriguingly resumed in *TLR9*$^{-/-}$ mice, which maintained a low number of parasites compared with the parasite load from WT mouse lesions (Supplemental Figure 3C). In this context, we speculate that an exacerbated compensatory inflammatory reaction is the main cause for tissue damage and edema rather than parasite replication itself.

To further investigate the role of TLR9 in the induction of CD200 expression in vivo, we removed the tissue lesions from mouse footpads and analyzed CD200 expression by flow cytometry. Total expression of CD200 was first analyzed in CD45$^{+}$ and CD45$^{-}$ cell populations obtained from WT and *TLR9*$^{-/-}$ mice (Figure 5E and Supplemental Figure 4, A–D). Double-positive (CD45$^{+}$CD200$^{+}$) cells were significantly higher in WT than in *TLR9*$^{-/-}$ cells recovered from the lesions (Figure 5F). The same results were obtained for CD45$^{-}$ and CD200$^{+}$ cells (Supplemental Figure 4E). Despite these differences in the absolute number of CD200-expressing cells between WT and *TLR9*$^{-/-}$, the mean fluorescence intensity (MFI) was similar, indicating that CD200 was equally detected in the 2 experimental groups (Figure 5G). More importantly, a marked difference was observed in the absolute number of macrophages (CD45$^{+}$CD11b$^{+}$F4/80$^{+}$ cells). WT mice contained 3-fold higher levels of macrophages than *TLR9*$^{-/-}$ mice (Figure 5H) and those cells

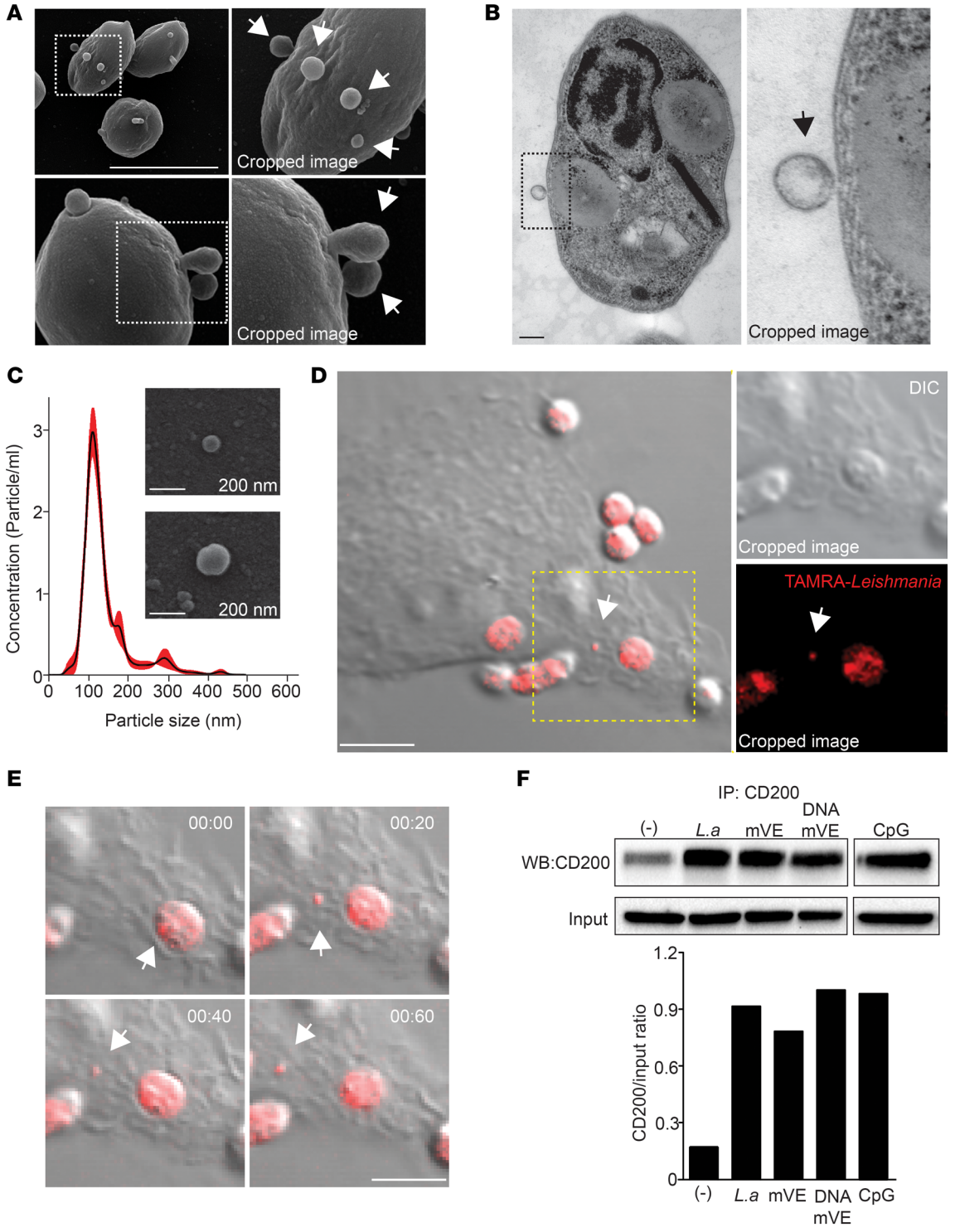


**Figure 4. *Leishmania amazonensis* amastigotes release DNA-containing EVs for CD200 induction.** (**A**) Scanning electron (SEM) and (**B**) transmission electron microscopy (TEM) images showing the mVEs (arrowheads) generated on the membrane of *L. amazonensis* amastigotes. Scale bars: 10 μm (**A**) and 200 nm (**B**). A cropped image is presented for best visualization. (**C**) Nanoparticle tracking analysis (NTA) shows the concentration (particles per ml) and the size (particle size in nm) of *L. amazonensis* mVEs. Representative image of 2 different mEVs visualized by SEM are shown (inset). (**D**) The time-lapse release of mEV-TAMRA from *L. amazonensis* amastigotes in infected BMMs recorded for 60 minutes and examined by confocal microscopy. Representative DIC/TAMRA fluorescence (red) image at 20 minutes of infection. (**E**) Right images show 4 merged pictures from the time-lapse video recorded for 60 minutes (see Supplemental Video 1). The white arrowhead shows an mVE released by amastigotes. Scale bars: 5 μm (**D** and **E**). (**F**) CD200 levels in BMMs incubated for 1 hour with parasites (*L.a*), parasite mVEs, or purified mVE-DNA. CpG was used as a positive control to induce CD200 expression. IP-input samples were verified by using actin levels as a loading control, which was used in the densitometric analysis (CD200/actin input ratio).

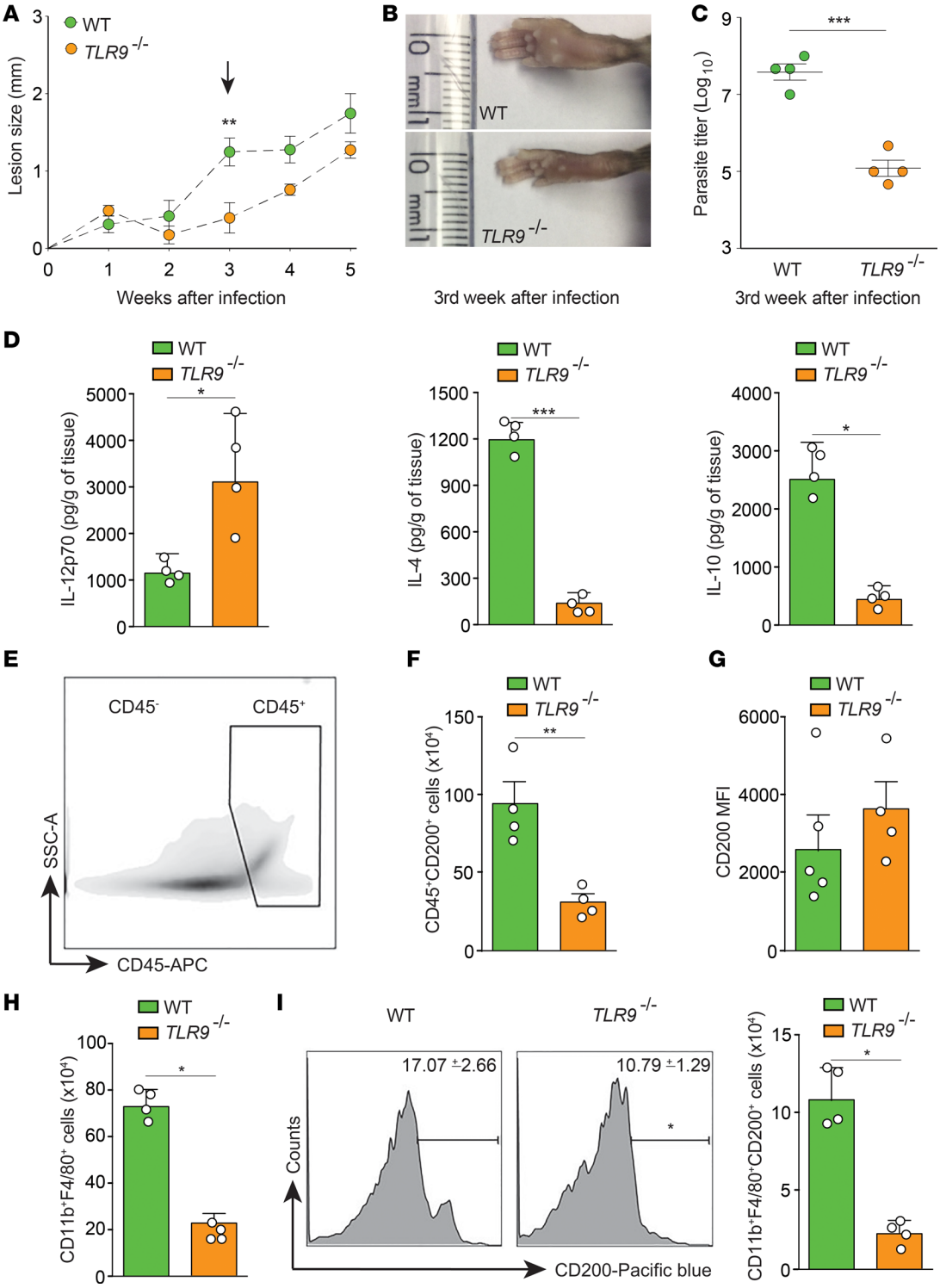


**Figure 5. Low virulence of *Leishmania amazonensis* in *TLR9*$^{-/-}$ mice is associated with reduced CD11b$^{+}$F4/80$^{+}$CD200$^{+}$ cells and proinflammatory cytokines in the lesion.** (**A**) Lesion size during the course of WT and *TLR9*$^{-/-}$ mouse infection with *L. amazonensis*. Results correspond to the mean ± SD ($n$ = 5). $^{**}P < 0.01$ (Student's $t$ test). (**B**) Representative image of the lesions generated at the left footpad in WT and *TLR9*$^{-/-}$ mice in the *L. amazonensis* infection experiment shown in **A**. (**C**) Parasite load in the footpads of WT and *TLR9*$^{-/-}$ mice infected with *L. amazonensis* at the third week of infection. Results correspond to mean ± SD ($n$ = 4). $^{***}P < 0.001$ (Student's $t$ test). (**D**) Cytokine profile of draining cells from footpad homogenates quantified by ELISA. Results correspond to the mean ± SD ($n$ = 4). IL-12p70, $^{*}P = 0.0106$; IL-4, $^{***}P < 0.001$; IL-10, $^{*}P < 0.0228$ (Student's $t$ test). (**E**) By flow cytometry, CD45$^{+}$ and CD45$^{-}$ cells from lesions were analyzed for CD200 expression in nonimmune (**F**) and immune cells (**G**). $^{*}P < 0.01$ (Student's $t$ test). (**H**) Total macrophages at the lesion site in WT and *TLR9*$^{-/-}$ mice infected with *L. amazonensis* and analyzed by flow cytometry. Results correspond to the mean ± SD ($n$ = 4). $^{*}P = 0.0106$ (Student's $t$ test). (**I**) Representative histograms used to calculate the percentage of CD200$^{+}$ macrophages and the absolute number of CD11b$^{+}$F4/80$^{+}$CD200$^{+}$ cells at the lesion site of WT and *TLR9*$^{-/-}$ mice infected with *L. amazonensis*. Results correspond to the mean ± SD ($n$ = 4). $^{*}P = 0.0114$ (Student's $t$ test).

expressed significantly more CD200 than the normalized number of macrophages from *TLR9*$^{-/-}$ mice (Figure 5I). These results would explain the low parasite burden in the lesions from *TLR9*$^{-/-}$ mice at the third week of infection.

A similar analysis was performed with samples of lymph nodes obtained from WT and *TLR9*$^{-/-}$ infected mice. The lymph nodes obtained from *TLR9*$^{-/-}$ infected mice were significantly smaller than WT mice (Figure 6A), and the expression levels of CD200 were lower than WT (Figure 6B). Notably, the levels of IL-1β, IL-12, and iNOS transcripts were significantly higher in *TLR9*$^{-/-}$ mice, showing no difference in IL-4 and IL-10 transcripts when compared to the WT mice (Figure 6C).

Collectively, the in vivo analyses indicate that TLR9 facilitates the progression of cutaneous lesions and parasite burden by inducing the expression of CD200, a ligand that inhibits the microbicidal activity of macrophages and other immune cells. Finally, we demonstrated that the impairment of CD200 expression in *TLR9*$^{-/-}$ mice reduces macrophage recruitment but increases the proinflammatory response of cytokines and iNOS in the lesions and lymph nodes. To the best of our knowledge, this is the first time that TLR9 has been directly associated with the induction of CD200 expression in *L. amazonensis* infection, and therefore this study represents what we believe is an entirely new mechanism of subversion of the innate immune response by *Leishmania* parasites.

## Discussion

*Leishmania* employs different functional mechanisms to evade macrophage defenses. Here, we identified TLR9 as a key component of the molecular machinery that induces CD200 through the MyD88/TRIF signaling pathway in macrophages infected by *L. amazonensis*. We further demonstrate that activation of TLR9 by parasite DNA enclosed in mVEs triggers a signaling pathway that culminates in CD200 expression and inhibition of iNOS and NO production. Finally, we show that the development of advanced lesions and the recruitment of inflammatory macrophages is impaired in TLR9-deficient mice during the early stages of the infection.

In this study, we show that TLR9 activation recruits 2 intracellular adaptor molecules, MyD88 and TRIF, which subsequently triggers intracellular signaling pathways that culminate with CD200 expression. The importance of MyD88 in TLR9 activation is well known (40), but only TRIF signaling is proposed to respond to high doses of CpG oligodeoxynucleotide (27). This could partially explain the differences in the CD200 inhibitory effect induced by the parasite and not by the TLR9 agonist. Although TLR9/TRIF signaling may act independently of MyD88 (27), our results suggest molecular crosstalk between MyD88 and TRIF to induce CD200 expression, regardless of the presence or activation of other TLRs. Activation of both adaptors has also been demonstrated in signaling cascades triggered by TLR4 in models of chronic diseases (41). Curiously, treatment with CD200-Fc suppresses the expression of TLR4 in macrophages (42), and noninfected *TLR4*$^{-/-}$ mouse–derived macrophages have a high expression of CD200 (Figure 2B); it is tempting to speculate that during *L. amazonensis* infection, TLR9 counterbalances TLR4 activation. Further studies are required to clarify this hypothesis.

In *Leishmania* spp., shedding of EVs can inhibit the host cell response (33, 36). Our results suggest that TLR9 activation by live intracellular amastigotes of *L. amazonensis* is dependent on the release of mVEs containing specific DNA sequences inside the macrophage parasitophorous vacuole. TLR9 located in the endoplasmic reticulum (43, 44) traffics through the Golgi complex (45) for relocation and activation in acidified intracellular compartments (46, 47). *L. amazonensis* amastigotes reside within acidic parasitophorous vacuoles with lysosomal properties (48) formed with membrane contributions derived from the endoplasmic reticulum (49). We suspect that these properties can promote the rapid recruitment of TLR9. Vesicle shedding from the parasite surface is stimulated under specific conditions such as elevated temperature or contact with host molecules (50). Based on this evidence, we propose that mVEs are likely released from the surface of intracellular amastigotes inside the parasitophorous vacuole and immediately activate TLR9/MyD88/TRIF signaling pathways. Moreover, intact mVEs may also break during contact with lysosomal enzymes, which would release vesicular content into the *Leishmania* parasitophorous vacuole, leading to a further level of analytical complexity.

In vivo, we showed that the reduction of CD200 at the site of lesions affects its progression with consequent reduction of inflammation in the proximal lymph nodes of *TLR9*$^{-/-}$ infected mice. One might suggest that such results are temporal and restricted to the early phase of *L. amazonensis* infection in which we detected an antiinflammatory-like immune response (IL-12$^{lo}$, IL-10$^{hi}$, IL-4$^{hi}$), which correlates with the

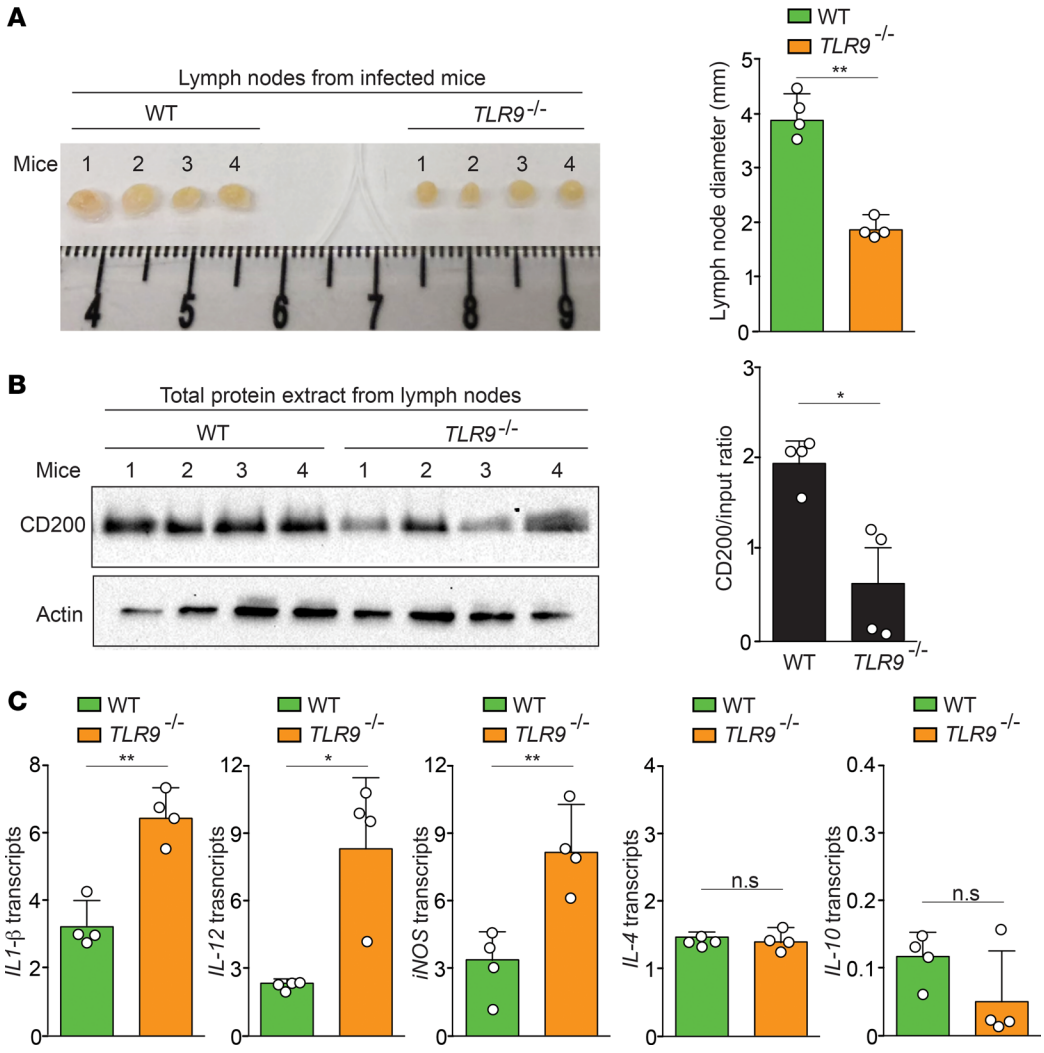


**Figure 6. TLR9-mediated CD200 expression is critical for the antiinflammatory environment in draining lymph nodes during *Leishmania amazonensis* infection.** (**A**) Representative image and quantification of the diameter size of lymph nodes from WT and *TLR9*$^{-/-}$ mice infected by *L. amazonensis*. Results correspond to the mean ± SD ($n$ = 4). $^{**}P < 0.0012$ (Student's $t$ test). (**B**) CD200 expression levels of the lymph nodes shown in **A**, with the densitometric analysis of the CD200/actin ratio. The data correspond to the mean ± SD ($n$ = 4). $^{**}P < 0.0108$ (Student's $t$ test). (**C**) Cytokine profile of the draining cells from the infected lymph nodes quantified by qPCR. Results correspond to the mean ± SD ($n$ = 4). IL-1β, $^{**}P < 0.0017$; IL-12, $^{*}P < 0.0146$; iNOS, $^{**}P < 0.0061$; IL-4, n.s. $P = 0.6431$; IL-10, n.s. $P = 0.1589$ (Student's $t$ test).

TLR9-mediated CD200 phenotype. At the fifth week of infection, however, the sizes of lesions in *TLR9*$^{-/-}$ mice are comparable to those in WT mice. Because the lesions from *TLR9*$^{-/-}$ mice showed a low number of parasites compared with the parasite load from WT mice (Supplemental Figure 3C), we speculate that an exacerbated antiinflammatory reaction is the main cause of tissue damage and edema rather than parasite replication itself. Notably, it was reported that deficiency of several TLRs, including TLR9, increased edema and fibrosis in a surgical model if lymphedema (51), supporting our results. Thus, in the absence of CD200 expression in our *Leishmania* infection model, the local immune response is unbalanced, favoring the recruitment of more proinflammatory cells that on one hand inhibits parasite growth, and on the other hand modulates healing of the damaged tissue, a process that is associated with chronic infection (52).

Contrary to our observations, TLR9 has been associated with control of parasite growth in infections with *Leishmania braziliensis* (53) and *Leishmania major* (54). These differential capacities to activate TLR9 may partially explain the marked virulence disparity of several *Leishmania* species in different hosts. Indeed, in humans, *L. braziliensis* and *L. major* can lead to mucocutaneous and mild cutaneous forms of leishmaniasis, respectively. However, the presence of recombinant CD200-Fc in lesions caused by *L. major,* which

cannot induce CD200 expression in macrophages, transformed these parasites into virulent pathogens that generate nonhealing, advanced lesions in vivo (11). Perhaps the ability to induce CD200 through TLR9/MyD88/TRIF signaling is the critical factor that could explain the opposite function of TLR9 in the susceptibility of *L. major* infection in TLR9-deficient mice (55) or the proper activation of innate immunity of NK cells against *Leishmania infantum chagasi* infection (56), in which models only TLR9/MyD88 signaling has been explored.

In conclusion, we show that TLR9 regulates macrophage activation by linking TLRs and intracellular parasites to induce CD200 expression by *L. amazonensis*. Our findings demonstrate that CD200-mediated signaling is markedly reduced in *TLR9*$^{-/-}$. Of note, it is important to be cautious regarding the TLR-mediated signaling pathway and iNOS/NO mechanism among species, particularly mouse and human. For instance, it was suggested that LPS and IFN-γ do not efficiently induce iNOS and NO in human macrophages (57), and the expression of TLR9 seems to be restricted to some human myeloid cells (58), as opposed to all myeloid cells in mice. In a mechanistic context, the work presented here provides an experimental blueprint for how host genetic composition influences *Leishmania* virulence.

## Methods

*Leishmania culture, purification, and mouse models*. *L. amazonensis* (IFLA/BR/67/PH8) were propagated as promastigotes at 26°C in M199 media containing 5% penicillin/streptomycin, 0.1% hemin (25 mg/ml in 0.1N NaOH), 10 mM adenine, and 10% fetal bovine serum (FBS), at pH 7.4. To generate axenic amastigotes, stationary-phase promastigote cultures (which are enriched in metacyclic promastigotes) were incubated at 2 × 10$^6$/ml in M199 media containing 0.25% glucose, 0.5% trypticase, 40 mM sodium succinate (at pH 4.5), 20% FBS, and 5% penicillin/streptomycin at 32°C for a minimum of 6 days, and then cultured axenically at 32°C. Parasites were washed 3 times in phosphate-buffered saline (PBS) before use in experiments. To obtain lesion amastigotes, female C57BL/6 mice were infected in the left hind footpad with 1 × 10$^6$ *L. amazonensis* stationary-phase promastigotes. After 4–5 weeks, the animals were killed, and the parasites recovered from footpad lesions as described previously (5). The lesion homogenate rich in amastigotes was submitted to sequential centrifugation steps at 2,000 *g* to separate parasites from tissue debris.

Six- to eight-week-old C57BL/6 WT female mice and *MyD88*$^{-/-}$, *TRIF*$^{-/-}$, *TLR2*$^{-/-}$, *TLR3*$^{-/-}$, *TLR4*$^{-/-}$, and *TLR9*$^{-/-}$ (all presenting C57BL/6 background) were bred and maintained in the animal facility of the Department of Parasitology at the Institute of Biomedical Sciences, University of São Paulo. *TLR2*$^{-/-}$, *TLR3*$^{-/-}$, *TLR4*$^{-/-}$, and *TLR9*$^{-/-}$ mice were provided by Dario Zamboni (Department of Biochemistry and Immunology, School of Medicine of Ribeirão Preto, University of São Paulo, Brazil).

*Mouse infection and quantification of parasite load*. WT and *TLR9*$^{-/-}$ mice were injected in the left hind footpad with 1 × 10$^6$ *L. amazonensis* stationary-phase promastigotes and lesion progression was followed by blinded weekly measurements with a caliper. The total number of parasites in the injected footpad was estimated by a limiting dilution assay as previously described (11) with some modifications. Footpad tissue homogenates were dissociated by incubation with collagenase (2 mg/ml, Sigma-Aldrich) in Tyrode buffer (140 mM NaCl, 5 mM KCl, 2.5 mM $CaCl_2$, 10 mM HEPES, 2 mM $MgCl_2$, pH 7.2) for 2 hours at 37°C under mild agitation. After collagenase dissociation, the homogenate was filtered in a Falcon 70-mm pore-size cell strainer (Corning), centrifuged at 20 *g* for 5 minutes, and washed 2 times with PBS (230 *g*, 10 minutes). The supernatant was used for cytokine quantification and the cellular pellet was suspended in 1 ml of PBS for further analyses by flow cytometry and parasite load quantification by limiting dilution. For parasite limiting dilution assays, the cell suspension was diluted 100-fold in complete M199 media, and then a 10-fold serial dilution in 96-well plates was performed. The number of viable parasites was calculated after 10 days from the highest dilution in which promastigote growth was observed. Results are presented as the $\log_{10}$ of the dilution (11).

*BMMs, treatments, and in vitro infection*. BMMs were prepared as described previously (11). Briefly, BMMs from mice were obtained after 7 days of differentiation of bone marrow in RPMI 1640 media (Gibco, Invitrogen) supplemented with 20% (v/v) FBS and 20% (v/v) L-929 cell supernatant. For macrophage infection, 2 × 10$^6$ (protein extracts) or 2 × 10$^5$ (IF) BMMs were plated in 6-well or 24-well dishes, respectively, 24 hours prior to experiments. For IF, BMMs were plated on glass coverslips in dishes. Lesion amastigotes were added at a multiplicity of infection (MOI) of 2 in RPMI supplemented with 10% (v/v) FBS and 2% (v/v) L-929 cell supernatant for 1 hour at 34°C. BMMs were then washed 3 times with PBS and incubated for the indicated times.

In some experiments, BMMs were incubated with different molecules, such as PGN, poly I:C, LPS, CpG oligodeoxynucleotides (Invivogen), at 1 μg/ml for 1 hour. In other experiments, BMMs were stimulated with different concentrations of total DNA of *L. amazonensis* amastigotes for 1 hour. The parasite DNA (RNA and protein free) was extracted with the GenElute Kit (Sigma-Aldrich) as instructed by the manufacturer. After incubation with different stimuli, cell samples were obtained for protein extraction by using Pierce IP lysis buffer (Thermo Fisher Scientific) with protease inhibitor cocktail (Thermo Fisher Scientific). For quantification of in vitro infection, coverslips containing the infected cells were fixed in PBS containing 4% PFA, washed with PBS and prepared for IF. For each experiment, at least 300 cells per coverslip were counted for each assay.

*In vitro phagocytosis/viability assays and IF*. To verify the importance of amastigote internalization and viability on CD200 induction, we performed the following pretreatment before infection assays. BMMs were pretreated with Cyto-D (Sigma-Aldrich) at 2 μM for 30 minutes at 37°C. To analyze amastigote viability on CD200 induction, parasites were kept in medium (Alive group) and treated with PBS containing 4% PFA for 10 minutes (PFA group) or inactivated by heat at 65°C for 45 minutes (Heat group). After the different treatments, the samples were washed in PBS, followed by parasite infection (MOI = 2) for 1 hour. After infection, the samples were washed and processed for IF or IP/Western blot. For IF, the samples were fixed with PBS containing 4% PFA and processed without permeabilization to recognize attached (detected by polyclonal anti-*Leishmania* antibodies) and internalized (not detected by polyclonal anti-*Leishmania* antibodies) parasites. Briefly, PFA-fixed cells in coverslips were washed with PBS, quenched with 50 mM $NH_4Cl$ for 15 minutes prior to staining with rabbit polyclonal antibodies prepared against amastigotes of *L.* (*L.*) *amazonensis*, followed by anti–rabbit IgG Alexa Fluor 488 (Molecular Probes). Samples were incubated with 10 μg/ml propidium iodide (Sigma-Aldrich) to detect the nuclei of all parasites and host cells. The images were acquired in a fluorescence microscope (Leica DMI6000B/AF6000) coupled to a digital camera system (DFC 365 FX, Leica) and processed by the Leica Application Suite X (LAS X) and ImageJ software (59). Quantification of the infection was made by counting a minimum of 300 cells per coverslip, with technical and biological triplicates. Results were expressed as number of parasites per 100 infected macrophages or percentage of infected macrophages.

*Time-lapse imaging*. *L. amazonensis* axenic amastigotes were washed 3 times in PBS (200 *g*, 10 minutes) and incubated with TAMRA-SE (5 μM) and Hoechst (2.5 μM) for 1 hour at 34°C. TAMRA-loaded parasites were washed several times to discard any extracellular fluorescent marker and incubated on ice with BMM previously plated in MatTek 35-mm petri dishes containing 1.5 coverglass (MatTek Corporation). After 1 hour of cold incubation, the petri dishes were placed for time-lapse imaging on a fluorescence microscope (Leica DMI6000B/AF6000) coupled to a digital camera system (DFC 365 FX) and processed by Leica Application Suite X (LAS X) and ImageJ software.

*Western blot and IP*. A total of 20 μg of protein/well was resolved under reducing conditions in a 12% SDS polyacrylamide gel, blotted onto nitrocellulose membranes using a Trans-blot Transfer system (Bio-Rad) for 1–2 hours at 250 mA, and probed with rabbit anti–mouse iNOS mAb (Abcam) and rabbit anti–mouse actin mAb (Imuny-VBP Biotecnologia Ltda.) followed by peroxidase-conjugated secondary antibodies (Imuny-VBP Biotecnologia Ltda.). CD200 protein detection was performed using the Pierce Crosslink Immunoprecipitation Kit as instructed by the manufacturer (Thermo Fisher Scientific). Briefly, a total of 100 μg of protein/sample was added to columns containing goat anti–mouse CD200 antibodies (R&D Systems) crosslinked to protein A/G beads. After several washes, elution buffer (35 μl) was added. The eluate samples were resolved under reducing conditions in a 12% SDS polyacrylamide gel, blotted onto nitrocellulose membranes, and probed with goat anti-CD200 antibodies followed by peroxidase-conjugated secondary antibody. Immunoblots were developed by using the Supersignal West Pico Chemiluminescent Substrate (Thermo Fisher Scientific) and detected with a ChemiDoc Imaging System (Bio-Rad) and ImageLab (Bio-Rad) software. A complete list of the antibodies used in this study can be found in Supplemental Table 1.

*qPCR*. Lymph nodes were ground in a Medimachine (Becton Dickson) and mechanically dissociated using a pellet pestle in complete PBS. Tissue homogenates were filtered in a 70-μm pore-size cell strainer (Falcon Products, Inc.) and divided into 2 samples of protein extracts for Western blot/IP analysis and RNA isolation for qPCR. The RNA extraction and purification were performed using the Quick-RNA MiniPrep kit (Zymo Research) according to manufacturer specifications. Quantification was carried out in a NanoDrop instrument (Thermo Fisher Scientific) and the complementary deoxyribonucleic acid (cDNA)

synthesis was performed using the SuperScript III Reverse Transcriptase kit (Invitrogen). qPCR was performed in a StepOnePlus Real-Time PCR System (Applied Biosystems) using Maxima SYBR Green/ROX qPCR Master Mix (Thermo Fisher Scientific) according to the manufacturer's instructions. Oligonucleotide primers are presented in Supplemental Figure 4F. The reaction was incubated for 10 minutes at 95°C and then for 40 cycles of 15 seconds at 95°C, 30 seconds at 55°C, and 30 seconds at 72°C. Fluorescence was detected at each annealing step. Technical triplicates were performed for each reaction and negative controls were included. The data are presented as relative quantification normalized by the level of *Hprt1* expression, calculated using $2^{-\Delta\Delta Ct}$ (60).

*NO measurement*. BMMs were incubated with LPS at 500 ng/ml (Invivogen) for 6 hours at 37°C and 5% $CO_2$. After incubation, cells were washed 3 times with PBS and subjected to *L. amazonensis* infection or stimulated as indicated. BMMs in these conditions were incubated and maintained for 42 hours. Cells were processed for protein extraction, and the supernatant was centrifuged and filtered for nitrite quantification. Nitrite concentrations in BMMs culture supernatants were used as a measure of NO production and quantified by using a Measure-iT High-Sensitivity Nitrite Assay Kit (Thermo Fisher Scientific) as instructed by the manufacturer. The fluorescence signal was measured at 450 nm after excitation at 365 nm. The NO concentration in each sample was calculated from a standard calibration curve as instructed by the manufacturer.

*Isolation and characterization of EVs*. *L. amazonensis* axenic amastigotes were washed 3 times in PBS (200 *g*, 10 minutes), and a total of $1 \times 10^9$ parasites were incubated for 2 hours at 34°C in amastigote medium, which was previously filtered and ultracentrifuged at 100,000 *g* to eliminate vesicles from FBS, for EV release. Amastigotes were then removed by centrifugation (200 *g*, 10 minutes), fixed, and analyzed by SEM or TEM, as described previously (61, 62). EV-containing supernatants were filtered through a 0.45-μm sterile cell strainer and used for NTA characterization or incubation assays for CD200 induction in BMMs.

Size, distribution, and concentration of isolated vesicles were analyzed as described previously (63). Briefly, EVs in the supernatants were measured in a Nanosight NS300 instrument (Malvern Instruments Ltd) equipped with a 405-nm laser and coupled to a CCD camera (the laser emitting a 60-mW beam at 405-nm wavelength). Data were analyzed using the NTA software (version 2.3 build 0017). The detection threshold was set to 10. Blur, Min track Length, and Min Expected Particle Size were set to auto. To perform the measurements, samples were diluted 100-fold with PBS. Readings were taken in triplicate for 30 seconds at 20 frames per second, with the camera level set to 14 and manual monitoring of temperature (19°C). The EV purity was analyzed mainly by both the size of the released EVs (NTA) and by SEM of the vesicles released by the parasite.

Purified EVs or total shed material was used in BMM stimulation assays for CD200 induction. The filtered supernatants were centrifuged 100,000 *g*, 1 hour (rotor 70.1T, XL-100K Ultracentrifuge, Beckman Coulter) to concentrate the EVs, which were then resuspended in RPMI 1640 supplemented with 10% (v/v) filtered and ultracentrifuged FBS. In another set of experiments, DNA from mVEs (RNA and protein free) was extracted using the GenElute Kit (Sigma-Aldrich) as instructed by the manufacturer. After incubation with mVEs or VEs-DNA (1 μg/ml), BMMs were processed for CD200 detection by IF/Western blot as described previously (11).

*Cytokine analysis*. IL-1β, IL-4, IL-6, IL-10, IL-12p40, IL-12p70, IFN-γ, and TNF-α levels were determined with OptEIA ELISA sets (BD Biosciences). All analyses were performed according to the manufacturer's recommendations. Values were expressed as pg/g of lesion tissue deduced from standard curves of each recombinant cytokine.

*Flow cytometry*. Cells isolated from footpad lesions after collagenase digestion were counted, suspended in PBS containing 2% FBS and anti–mouse CD16/CD32 to block Fc receptors. Cells were then stained with fluorescence-conjugated antibodies for the surface markers CD45, CD11b, CD11c, MHC class II, F4/80, and CD200 (BD Biosciences) for 30 minutes at 4°C in the dark. After washes, cells were resuspended and transferred to polypropylene tubes (12 × 75 mm). Data were acquired in a FACSCanto II flow cytometer (BD Biosciences) and analyzed using FlowJo software, version 10.0.7 (Tree Star Inc.).

*Statistics*. Data were analyzed with commercial software (GraphPad Software Prism 6.0). Two-way ANOVA with Sidak's post hoc test was used when analyzing multiple groups. In some results, 1-way ANOVA with Tukey's post hoc test or 2-tailed Student's *t* test was used. *P* values of 0.05 or less were considered statistically significant. All experiments were repeated at least 3 times and representative data are presented, unless otherwise specified.

*Study approval*. All experiments were carried out in accordance with internationally recognized guidelines and in full agreement with local regulations (Brazilian Federal Law 11,794, Decree 6,899 and Normative Resolutions published by the National Council for the Control of Animal Experimentation [CONCEA]), and approved by the Institutional Animal Care and Use Committee (IACUC) of the University of São Paulo under protocol number 95/2013.

## Author contributions

IPS, DIS, and MC conceived and designed the project. IPS, KGM, MC, JBA, ASN, and ACT performed experiments. IPS, KGM, JBA, ASN, ACT, DIS, RP, WA, and MC analyzed data. IPS, DIS, RP, WA, and MC wrote and/or edited the manuscript. All authors read and agreed with the manuscript content.

## Acknowledgments

We thank Dario Zamboni (FMRP-USP) for the gift of *TLR*$^{-/-}$ mice, Mario Cruz (Imaging Core CEFAP-ICB-USP) for assistance with confocal microscopy, and Norma W. Andrews for critical discussions and review of the manuscript draft. We thank Brandi Mattson (Life Science Editors) for professional editorial services. This work was supported by FAPESP grant 2012/24105-3, CNPq Universal grant 443816/2014-0 (to MC), partially financed by CAPES- Finance Code 001, and by award from the Gillson-Longenbaugh Foundation (to RP and WA).

Address correspondence to: Mauro Cortez, Department of Parasitology, University of São Paulo, São Paulo, SP 05508. Brazil. Phone: 55.11.30917328; Email: mcortez@usp.br. Or to: Wadih Arap, Rutgers Cancer Institute of New Jersey and Division of Hematology/Oncology, Department of Medicine, Rutgers New Jersey Medical School, Newark, New Jersey 07730, USA. Phone: 281.701.0722; E-mail: wadih.arap@rutgers.edu.

1. Akira S. TLR signaling. *Curr Top Microbiol Immunol*. 2006;311:1–16.
2. Janeway CA, Medzhitov R. Innate immune recognition. *Annu Rev Immunol*. 2002;20:197–216.
3. Liu D, Uzonna JE. The early interaction of Leishmania with macrophages and dendritic cells and its influence on the host immune response. *Front Cell Infect Microbiol*. 2012;2:83.
4. Moradin N, Descoteaux A. Leishmania promastigotes: building a safe niche within macrophages. *Front Cell Infect Microbiol*. 2012;2:121.
5. Sacks DL, Melby PC. Animal models for the analysis of immune responses to leishmaniasis. *Curr Protoc Immunol*. 2001;Chapter 19:Unit 19.2.
6. Loeuillet C, Bañuls AL, Hide M. Study of Leishmania pathogenesis in mice: experimental considerations. *Parasit Vectors*. 2016;9:144.
7. Alvar J, et al. Leishmaniasis worldwide and global estimates of its incidence. *PLoS ONE*. 2012;7(5):e35671.
8. Hartley MA, Drexler S, Ronet C, Beverley SM, Fasel N. The immunological, environmental, and phylogenetic perpetrators of metastatic leishmaniasis. *Trends Parasitol*. 2014;30(8):412–422.
9. Teixeira DE, Benchimol M, Rodrigues JC, Crepaldi PH, Pimenta PF, de Souza W. The cell biology of Leishmania: how to teach using animations. *PLoS Pathog*. 2013;9(10):e1003594.
10. Silveira FT, Lainson R, De Castro Gomes CM, Laurenti MD, Corbett CE. Immunopathogenic competences of Leishmania (V.) braziliensis and L. (L.) amazonensis in American cutaneous leishmaniasis. *Parasite Immunol*. 2009;31(8):423–431.
11. Cortez M, Huynh C, Fernandes MC, Kennedy KA, Aderem A, Andrews NW. Leishmania promotes its own virulence by inducing expression of the host immune inhibitory ligand CD200. *Cell Host Microbe*. 2011;9(6):463–471.
12. Barclay AN, Wright GJ, Brooke G, Brown MH. CD200 and membrane protein interactions in the control of myeloid cells. *Trends Immunol*. 2002;23(6):285–290.
13. Gorczynski RM. CD200 and its receptors as targets for immunoregulation. *Curr Opin Investig Drugs*. 2005;6(5):483–488.
14. Yang Y, et al. Loss of neuronal CD200 contributed to microglial activation after acute cerebral ischemia in mice. *Neurosci Lett*. 2018;678:48–54.
15. Foster-Cuevas M, Wright GJ, Puklavec MJ, Brown MH, Barclay AN. Human herpesvirus 8 K14 protein mimics CD200 in down-regulating macrophage activation through CD200 receptor. *J Virol*. 2004;78(14):7667–7676.
16. Hoek RM, et al. Down-regulation of the macrophage lineage through interaction with OX2 (CD200). *Science*. 2000;290(5497):1768–1771.
17. Minas K, Liversidge J. Is the CD200/CD200 receptor interaction more than just a myeloid cell inhibitory signal? *Crit Rev Immunol*. 2006;26(3):213–230.
18. Aref S, Azmy E, El-Gilany AH. Upregulation of CD200 is associated with regulatory T cell expansion and disease progression in multiple myeloma. *Hematol Oncol*. 2017;35(1):51–57.
19. Elshal MF, Aldahlawi AM, Saadah OI, McCoy JP. Reduced dendritic cells expressing CD200R1 in children with inflammatory bowel disease: correlation with Th17 and regulatory T cells. *Int J Mol Sci*. 2015;16(12):28998–29010.
20. Liew FY, Millott S, Parkinson C, Palmer RM, Moncada S. Macrophage killing of Leishmania parasite in vivo is mediated by nitric oxide from L-arginine. *J Immunol*. 1990;144(12):4794–4797.

21. Wei XQ, et al. Altered immune responses in mice lacking inducible nitric oxide synthase. *Nature*. 1995;375(6530):408–411.
22. Casella JF, Flanagan MD, Lin S. Cytochalasin D inhibits actin polymerization and induces depolymerization of actin filaments formed during platelet shape change. *Nature*. 1981;293(5830):302–305.
23. Gurung P, Li B, Subbarao Malireddi RK, Lamkanfi M, Geiger TL, Kanneganti TD. Chronic TLR stimulation controls NLRP3 inflammasome activation through IL-10 mediated regulation of NLRP3 expression and caspase-8 activation. *Sci Rep*. 2015;5:14488.
24. Hemmi H, et al. A Toll-like receptor recognizes bacterial DNA. *Nature*. 2000;408(6813):740–745.
25. Sharma S, Fitzgerald KA, Cancro MP, Marshak-Rothstein A. Nucleic acid-sensing receptors: rheostats of autoimmunity and autoinflammation. *J Immunol*. 2015;195(8):3507–3512.
26. Troutman TD, Bazan JF, Pasare C. Toll-like receptors, signaling adapters and regulation of the pro-inflammatory response by PI3K. *Cell Cycle*. 2012;11(19):3559–3567.
27. Volpi C, et al. High doses of CpG oligodeoxynucleotides stimulate a tolerogenic TLR9-TRIF pathway. *Nat Commun*. 2013;4:1852.
28. Ahmad-Nejad P, Häcker H, Rutz M, Bauer S, Vabulas RM, Wagner H. Bacterial CpG-DNA and lipopolysaccharides activate Toll-like receptors at distinct cellular compartments. *Eur J Immunol*. 2002;32(7):1958–1968.
29. Rutz M, et al. Toll-like receptor 9 binds single-stranded CpG-DNA in a sequence- and pH-dependent manner. *Eur J Immunol*. 2004;34(9):2541–2550.
30. Jiang L, et al. CD200Fc reduces TLR4-mediated inflammatory responses in LPS-induced rat primary microglial cells via inhibition of the NF-κB pathway. *Inflamm Res*. 2016;65(7):521–532.
31. Atayde VD, et al. Leishmania exosomes and other virulence factors: Impact on innate immune response and macrophage functions. *Cell Immunol*. 2016;309:7–18.
32. Hassani K, Shio MT, Martel C, Faubert D, Olivier M. Absence of metalloprotease GP63 alters the protein content of Leishmania exosomes. *PLoS ONE*. 2014;9(4):e95007.
33. Silverman JM, et al. Leishmania exosomes modulate innate and adaptive immune responses through effects on monocytes and dendritic cells. *J Immunol*. 2010;185(9):5011–5022.
34. Kowal J, Tkach M, Théry C. Biogenesis and secretion of exosomes. *Curr Opin Cell Biol*. 2014;29:116–125.
35. Raposo G, Stoorvogel W. Extracellular vesicles: exosomes, microvesicles, and friends. *J Cell Biol*. 2013;200(4):373–383.
36. Hassani K, Olivier M. Immunomodulatory impact of leishmania-induced macrophage exosomes: a comparative proteomic and functional analysis. *PLoS Negl Trop Dis*. 2013;7(5):e2185.
37. Silverman JM, Reiner NE. Leishmania exosomes deliver preemptive strikes to create an environment permissive for early infection. *Front Cell Infect Microbiol*. 2011;1:26.
38. Atayde VD, Aslan H, Townsend S, Hassani K, Kamhawi S, Olivier M. Exosome secretion by the parasitic protozoan Leishmania within the sand fly midgut. *Cell Rep*. 2015;13(5):957–967.
39. Ji J, Sun J, Soong L. Impaired expression of inflammatory cytokines and chemokines at early stages of infection with Leishmania amazonensis. *Infect Immun*. 2003;71(8):4278–4288.
40. Rogers GL, et al. Unique roles of TLR9- and MyD88-dependent and -independent pathways in adaptive immune responses to AAV-mediated gene transfer. *J Innate Immun*. 2015;7(3):302–314.
41. Kim S, et al. Signaling of high mobility group box 1 (HMGB1) through toll-like receptor 4 in macrophages requires CD14. *Mol Med*. 2013;19:88–98.
42. Hayakawa K, et al. CD200 restrains macrophage attack on oligodendrocyte precursors via Toll-like receptor 4 downregulation. *J Cereb Blood Flow Metab*. 2016;36(4):781–793.
43. Latz E, et al. TLR9 signals after translocating from the ER to CpG DNA in the lysosome. *Nat Immunol*. 2004;5(2):190–198.
44. Takeshita F, et al. Cutting edge: Role of Toll-like receptor 9 in CpG DNA-induced activation of human cells. *J Immunol*. 2001;167(7):3555–3558.
45. Chockalingam A, Brooks JC, Cameron JL, Blum LK, Leifer CA. TLR9 traffics through the Golgi complex to localize to endolysosomes and respond to CpG DNA. *Immunol Cell Biol*. 2009;87(3):209–217.
46. Häcker H, et al. CpG-DNA-specific activation of antigen-presenting cells requires stress kinase activity and is preceded by non-specific endocytosis and endosomal maturation. *EMBO J*. 1998;17(21):6230–6240.
47. Latz E, et al. Ligand-induced conformational changes allosterically activate Toll-like receptor 9. *Nat Immunol*. 2007;8(7):772–779.
48. Antoine JC, Prina E, Jouanne C, Bongrand P. Parasitophorous vacuoles of Leishmania amazonensis-infected macrophages maintain an acidic pH. *Infect Immun*. 1990;58(3):779–787.
49. Ndjamen B, Kang BH, Hatsuzawa K, Kima PE. Leishmania parasitophorous vacuoles interact continuously with the host cell's endoplasmic reticulum; parasitophorous vacuoles are hybrid compartments. *Cell Microbiol*. 2010;12(10):1480–1494.
50. Yao C, Donelson JE, Wilson ME. Internal and surface-localized major surface proteases of Leishmania spp. and their differential release from promastigotes. *Eukaryotic Cell*. 2007;6(10):1905–1912.
51. Zampell JC, et al. Toll-like receptor deficiency worsens inflammation and lymphedema after lymphatic injury. *Am J Physiol, Cell Physiol*. 2012;302(4):C709–C719.
52. Nylén S, Eidsmo L. Tissue damage and immunity in cutaneous leishmaniasis. *Parasite Immunol*. 2012;34(12):551–561.
53. Weinkopff T, et al. Role of Toll-like receptor 9 signaling in experimental Leishmania braziliensis infection. *Infect Immun*. 2013;81(5):1575–1584.
54. Liese J, Schleicher U, Bogdan C. TLR9 signaling is essential for the innate NK cell response in murine cutaneous leishmaniasis. *Eur J Immunol*. 2007;37(12):3424–3434.
55. Abou Fakher FH, Rachinel N, Klimczak M, Louis J, Doyen N. TLR9-dependent activation of dendritic cells by DNA from Leishmania major favors Th1 cell development and the resolution of lesions. *J Immunol*. 2009;182(3):1386–1396.
56. Schleicher U, et al. NK cell activation in visceral leishmaniasis requires TLR9, myeloid DCs, and IL-12, but is independent of plasmacytoid DCs. *J Exp Med*. 2007;204(4):893–906.
57. Weinberg JB. Nitric oxide production and nitric oxide synthase type 2 expression by human mononuclear phagocytes: a review. *Mol Med*. 1998;4(9):557–591.

58. Trevani AS, et al. Bacterial DNA activates human neutrophils by a CpG-independent pathway. *Eur J Immunol*. 2003;33(11):3164–3174.
59. Schneider CA, Rasband WS, Eliceiri KW. NIH Image to ImageJ: 25 years of image analysis. *Nat Methods*. 2012;9(7):671–675.
60. Livak KJ, Schmittgen TD. Analysis of relative gene expression data using real-time quantitative PCR and the 2(-delta delta C(T)) Method. *Methods*. 2001;25(4):402–408.
61. Corrotte M, et al. Caveolae internalization repairs wounded cells and muscle fibers. *Elife*. 2013;2:e00926.
62. Ribeiro KS, et al. Proteomic analysis reveals different composition of extracellular vesicles released by two . *J Extracell Vesicles*. 2018;7(1):1463779.
63. Nogueira PM, et al. Vesicles from different Trypanosoma cruzi strains trigger differential innate and chronic immune responses. *J Extracell Vesicles*. 2015;4:28734.